J. Eur. Opt. Society-Rapid Publ. 2024, **20**, 19

https://doi.org/10.1051/jeos/2024017
Available online at: https://jeos.edpsciences.org

EOSAM 2023
Guest editors: Patricia Segonds, Guy Millot and Bertrand Kibler

Journal of the European Optical Society-Rapid Publications

RESEARCH ARTICLE OPEN ACCESS

Towards 2-μm comb light source based on multiple four-wave mixing in a dual-frequency Brillouin fiber laser

Moise Deroh[1,2,*], Gang Xu[1,3], Erwan Lucas[1], Jean-Charles Beugnot[2], Hervé Maillotte[2], Thibaut Sylvestre[2], and Bertrand Kibler[1]

[1] Laboratoire Interdisciplinaire Carnot de Bourgogne, UMR 6303 CNRS, Université de Bourgogne, Dijon, France
[2] Institut FEMTO-ST, UMR 6174 CNRS, Université Franche-Comté, Besançon, France
[3] School of Optical and Electronic Information, Huazhong University of Science and Technology, Wuhan, PR China

Received 29 January 2024 / Accepted 5 April 2024

Abstract. In this study, we report the generation of multi-wavelength light sources through enhanced four-wave-mixing processes using a straightforward and adaptable dual-frequency Brillouin fiber laser. This passive optical and nonreciprocal cavity is first tested and analyzed with long fiber lengths up to 1 km in the 1.55 μm telecommunication C band and then in the 2-μm waveband. In the latter case, we demonstrate that our fiber cavity enables efficient multiple four-wave mixings, in the continuous-wave regime, which are commonly inaccessible in long silica-fibers due to increased losses. We also report on the tunable repetition rate from tens of GHz to hundreds of GHz, by simply changing the frequency spacing between the two continuous-wave pumps. The coherence limitations of our all-fiber system are discussed, along with the impact of the dispersion regime of the nonlinear fiber that forms the cavity.

Keywords: Stimulated Brillouin Scattering, Fiber cavities, Four-wave mixing, Frequency combs.

1 Introduction

Compact and coherent comb light sources in the 2-μm waveband are becoming attractive components for molecular spectroscopy, environmental monitoring, and next-generation high-speed optical communications [1–6]. Coherent comb light sources can be obtained in general through various optical configurations such as electro-optic modulation schemes and mode-locked pulsed lasers often assisted by additional nonlinear frequency conversion [7–11], and parametric oscillations from a continuous-wave (CW) laser in high quality factor microresonators [12, 13]. Mostly, developed systems focused on the telecommunication wavelength around 1.55 μm, thus benefiting from the numerous high-quality optical components. In the specific 2-μm waveband, common approaches typically involve near-infrared to mid-infrared conversion techniques of frequency combs and mode-locked lasers [3, 14, 15]. Alternately, other systems may be implemented using thulium (Tm)-doped silica fiber lasers and components or semiconductor lasers [2]. It is also worth mentioning that multi-wavelength fiber lasers have been developed around 2 μm using distinct cavity arrangements based on Tm-doped fibers [16–20].

In general, direct generation of comb light sources in the 2-μm waveband remains challenging in a cavity-free configuration with CW pumping, for instance, due to the detrimental losses in the required long optical fiber lengths (typically, tens of dB/km). As a consequence, multiple four-wave mixing (MFWM) processes in the simultaneous propagation of two pump waves through an optical fiber cannot be simply applied as in the conventional telecommunication window [21], even if bi-chromatic pumping allows for FWM to be free of power threshold. However, another alternative for generating combs has recently emerged by combining Kerr and Brillouin effects with the aim of improving some nonlinear performances. Indeed, stimulated Brillouin Scattering (SBS) can manifest with several orders of magnitude stronger than the Raman or Kerr effect, and it is also tunable over a wide spectral range [22]. Then one can excite and enhance MFWM processes in a non-reciprocal fiber cavity platform featuring bi-chromatic Brillouin lasing [23]. Direct coherent pumping is replaced by lasing on specific cavity modes, offering easily adjustable repetition rates and enhanced coherence by Brillouin purification [24]. A similar approach can be applied for generating a Kerr comb in an optical microresonator, using the Brillouin laser generated in the same cavity [25]. Highly coherent combs were also demonstrated in short fiber cavities by finely controlling the bi-chromatic Brillouin lasing [24].

* Corresponding author: koffi.deroh@u-bourgogne.fr

Table 1. Physical parameters at 1550 nm of the cavities study made of two distinct HNLFs in this work.

Fiber cavity parameters	Cavity 1	Cavity 2	Units
Cavity length (L)	350	1000	m
Brillouin gain efficiency (g_B/A_{eff})	0.38	0.38	$m^{-1}\cdot W^{-1}$
Brillouin gain bandwidth ($\Delta\nu_B$)	55	55	MHz
Total roundtrip loss	1.5	2.2	dB
Zero dispersion wavelength (λ_0)	1575	1523	nm
Dispersion parameter (D)	−2.95	0.49	$ps\cdot nm^{-1}\cdot km^{-1}$
Group-velocity dispersion (β_2)	3.77	−0.62	$ps^2\cdot km^{-1}$
Nonlinear coefficient (γ)	12.5	10	$W^{-1}\cdot km^{-1}$
Free spectral range (FSR)	0.6	0.22	MHz
Cavity finesse	8.69	5.94	–

In this paper, we investigate two multi-line fiber laser sources centered at 1.55 μm (C-band) and 2-μm (thulium band) that exhibit a symmetrical spectral comb structure based on enhanced MFWM within a long passive fiber cavity platform, specifically designed for bi-chromatic Brillouin lasing. At 1.55 μm, we generate a multi-wavelength light source that operates in both dispersion regimes with distinct temporal and spectral features. Temporal characterization of the generated pulse train is provided by means of intensity autocorrelation measurements. Finally, at 2 μm, we demonstrate a multi-wavelength light source made of 22 comb lines operating in the anomalous dispersion regime with a frequency spacing up to 106 GHz. The stability and coherence of the multi-line sources and generated pulse trains are also discussed for the two pumping configurations.

2 Experimental setup

In our experiments, we analyzed two distinct cavities made of commercially available highly nonlinear fibers (HNLF) that exhibit a normal and anomalous dispersion. The main physical parameters of both cavities are summarized in Table 1. Figure 1 shows the experimental setup used for generating our multi-wavelength sources in both spectral bands, namely 1.55 and 2 μm. The bi-chromatic pumping configuration can be achieved by combining two wavelength-tunable CW lasers (external cavity laser diodes) or by means of electro-optical (intensity) modulation (EOM) of one laser, to vary the pump frequency spacing [24]. Here, we chose two CW lasers to investigate larger frequency spacings. The two pump lasers were amplified via an erbium or thulium-doped fiber amplifier (EDFA/TDFA) and then injected into the passive fiber cavity via an optical circulator (OC). The backscattered Brillouin signals coming back from the FUT, shifted at the Brillouin frequency around 9.6 GHz [24] and 7.5 GHz [26] at 1.55 and 2 μm, respectively from our HNLF fibers, are then reinjected into the cavity ring via a fiber coupler (99:1). The output of the dual-frequency Brillouin fiber laser is extracted from a 1% fiber coupler while the remaining 99% is fed back into the ring cavity. An OC closes the ring cavity. This configuration system allows free propagation of the Stokes waves, which perform multiple roundtrips in the counterclockwise direction (dual lasing occurs and initiates a cascade of FWM), while the pumps waves interact only over a single pass in the clockwise direction. We finally analyzed the output cavity spectrum using an optical spectrum analyzer (with 0.08 pm and 0.05 nm resolution, at 1.55 and 2 μm respectively) and a rapid scanning intensity autocorrelator. In order to maximize the efficiency of the cascaded FWM processes, polarization controllers are inserted between the pumping lasers and the couplers to ensure that the two pumps have the same polarization direction. Specific fiber components dedicated to the 1.55- or 2-μm spectral bands can be easily interchanged.

3 Experimental results at 1.55 μm

In the following, our experiments were first performed at 1.55 μm with the first cavity made of the normally-dispersive HNLF. We first measured the output dual-frequency Brillouin laser power as a function of injected pump power, as shown in Figure 2a, and for a given frequency spacing of 25 GHz. A low lasing threshold of 7.5 mW was experimentally achieved. For a 25-GHz (0.2 nm) frequency spacing and 158-mW pump power, we specifically show the multi-line spectrum that was obtained in both open and closed cavity configurations as depicted in Figures 2a and 2c. Note that FWM processes occur and are analyzed in the clockwise direction in the particular open-cavity configuration, since there is no Brillouin Stokes lasing. The enhanced efficiency of the cascaded FWM process in a closed cavity is evident when driven by the Brillouin Stokes. This results in a notable increase, transitioning from a limited number of comb lines to a substantial expansion, reaching dozens. Figure 2d shows the resulting spectral evolution by increasing the injected pump power from 80 to 316 mW in the closed cavity case. The number of comb lines increases significantly; however, the overall spectral shape exhibits an exponential decay when the pump power increases. This rapid decline in power per line can be attributed to both the strong normal cavity dispersion and also the multimode Brillouin lasing regime for such

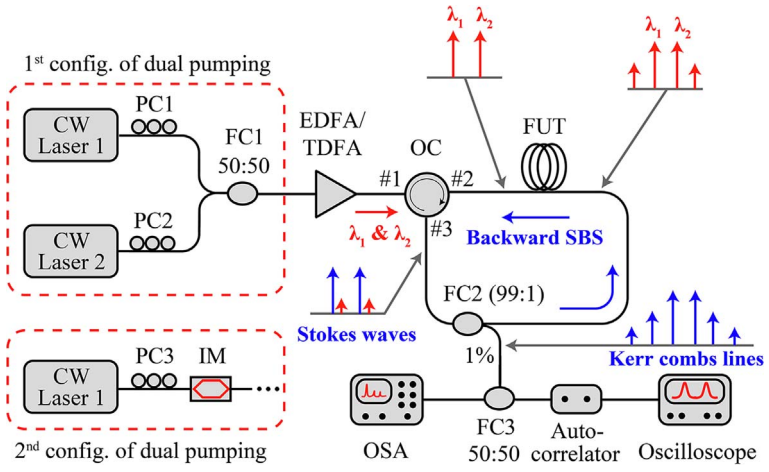

Fig. 1. Experimental setup for generating multi-wavelength light sources at both 1.55 μm and 2 μm by means of MFWM in a dual-frequency Brillouin fiber laser. CW: Continuous wave, PC: Polarization Controller, FC: Fiber Coupler, EDFA/TDFA: Erbium/Thulium Doped Fiber Amplifier, OC: Optical Circulator, FUT: Fiber Under Test, OSA: Optical Spectrum Analyzer.

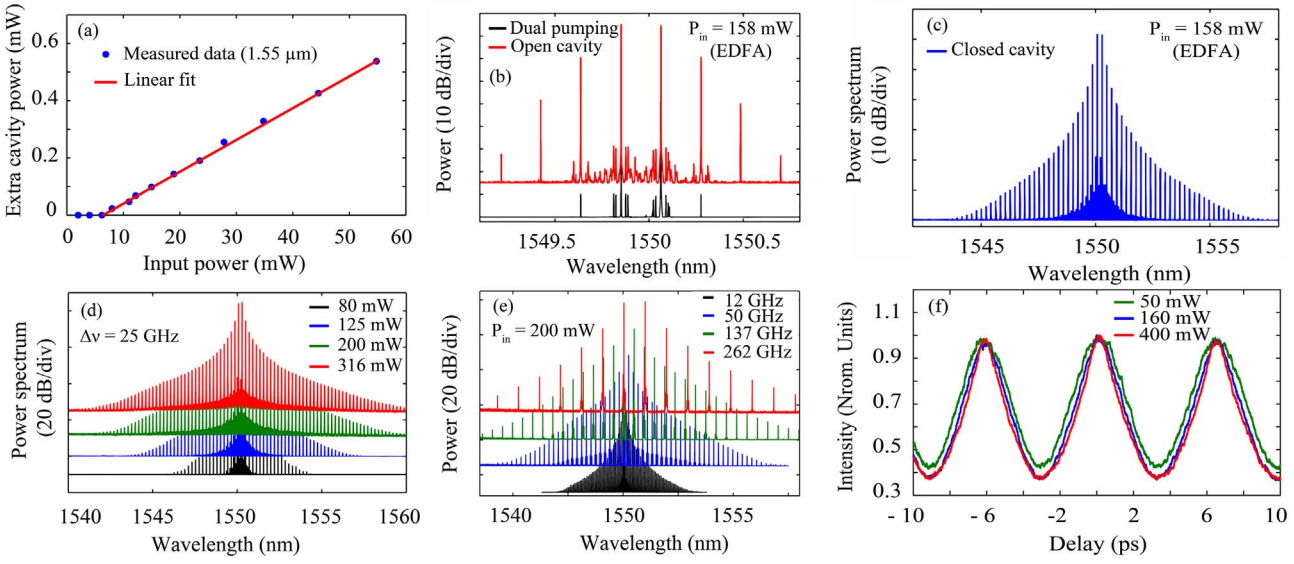

Fig. 2. Dual-frequency Brillouin laser and multi-wavelength light generation (cavity 1, normal dispersion regime). (a) Stokes lasing threshold measurement. (b) Experimental FWM results for bi-chromatic pumping (25-GHz frequency spacing) of the HNLF and cavity-free configuration for an input power of 158 mW. (c) Corresponding multi-wavelength generation in the closed cavity configuration. (d) Spectral broadening recorded (25-GHz frequency spacing) at increasing input pump powers from 80 to 316 mW. (e) Tunable frequency spacing of the multi-wavelength source for an input power of 200 mW. (f) Experimental autocorrelation traces of the generated pulse train with a period of 6.7 ps (repetition rate of 150 GHz) for distinct input powers of 50–400 mW.

long cavity length and high operating power [24]. Operating the Stokes laser in the multimode regime leads to a strong degradation in comb coherence as the Stokes pumps fluctuate across several cavity modes. Moreover, the thermal drift of our cavity relative to the pump lasers is not counterbalanced by any phase-lock loop, contrary to our previous work on a very short cavity [24]. As a result, our measurements only reflect a strong averaging of spectral broadening in the presence of pump power and cavity detuning fluctuations. Nevertheless, we show that the generated comb source can be tuned over a few hundreds of GHz by simply modifying the initial frequency spacing of the two CW pumps. We measured the dependence of the output cavity spectrum as a function of the frequency spacing for a given input power of 200 mW in Figure 2e. More particularly, we increased the pump frequency spacing from 12.5 to 262 GHz (0.1–2.1 nm). The spectral bandwidth of the generated comb lines exhibits rapid expansion up to a saturation point, accompanied by a decrease in the number of lines. This behavior is attributed to the inherent dispersion of the fiber, which restricts the spectral broadening, or, in other words, the maximum steepening of the

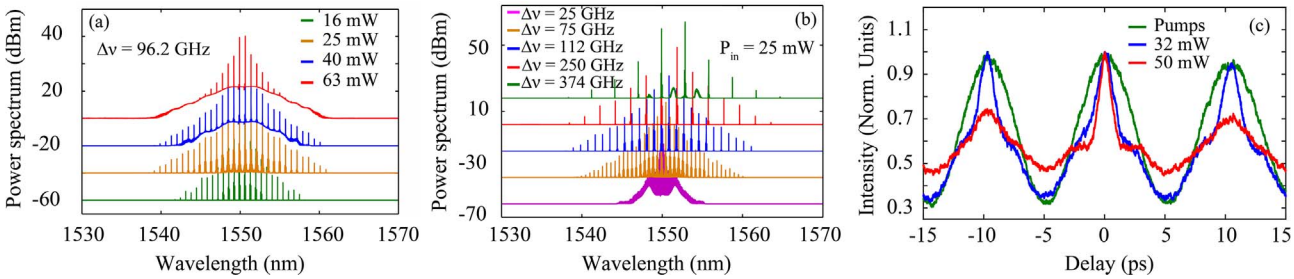

Fig. 3. Dual-frequency Brillouin laser and multi-wavelength light generation (cavity 2, anomalous dispersion regime). (a) Experimental FWM results for bi-chromatic pumping (96.2 GHz frequency spacing) of the HNLF and increasing input powers from 16 to 63 mW. (b) Tunable frequency spacing (from 25 GHz to 374 GHz) of the multi-wavelength source for an input power of 25 mW. (c) Experimental autocorrelation traces of the generated pulse train with a period of 10.4 ps (rep. rate of 96.2 GHz) for input powers of 32 to 50 mW.

temporal pulse fronts originating from the initial sinusoidal modulation induced by the two pumps [27]. Indeed, we characterized the temporal properties of the multi-wavelength spectrum with frequency spacing of 150 GHz for distinct pump powers, by means of a second-harmonic autocorrelator with a resolution of 10 fs (see Fig. 2f).

Under normal cavity dispersion, the initial sinusoidal temporal pattern resulting from the interference of the two Stokes fields in the cavity becomes a near-rectangular pulse train for increasing powers associated with larger spectral broadenings, as confirmed by the triangular waveform of the autocorrelation profile with a period of 6.7 ps.

Next, we carried out experiments with the second cavity made of the 1-km-long HNLF operating in the anomalous dispersion. We measured the spectral evolution of the output cavity for a given frequency spacing of 96.2 GHz (0.77 nm) and increased input powers from 16 to 63 mW (see Fig. 3a). In this dispersion regime, we once again observe the generation of a multi-wavelength light source; however, the spectral broadening experiences swift saturation at moderate powers, typically above 25 mW. Subsequently, a pronounced increase in the noise background becomes evident, creating a substantial pedestal beneath the comb lines. This distinct characteristic of the anomalous dispersion regime is closely related to the growth of modulation instability (MI) sidelobes. This adverse phenomenon, detrimental to coherence properties, was also observed in short fiber cavities [27]. However, it was successfully mitigated by employing suitable detuning conditions, resulting in the formation of a globally coherent comb. By contrast, the MI here prevents the growth of the combs lines in our long free-running cavity. In this case, it is important to avoid the MI effect. To this end, we restricted the input power to values below 25 mW. We then noticed that the MI emergence also depends on the frequency spacing between the two pumps. Figure 3b shows the output spectra obtained with different frequency spacings for an input power of 25 mW. We significantly increased the pump frequency spacing from 25 to 373.9 GHz (0.2–3.0 nm). We clearly confirm that the comb repetition rate can be easily tuned over a few hundreds of GHz. However, we note that MI sidelobes appear only for small or large frequency spacings (below 75 GHz or beyond 250 GHz). For a small frequency spacing, MI amplifies the noise under the overall MFWM spectrum, while MI sidelobes emerge between comb lines for a large frequency detuning. In between, when the pump frequency spacing is close to the MI offset frequency, the detrimental impact of MI remains negligible, at least for such a power. Indeed, in Figure 3c, we provide the temporal autocorrelation traces of the multi-wavelength source generated with 96.2-GHz frequency spacing (0.77 nm) for several pump powers.

We found that the initial sinusoidal pattern with a period of 10.4 ps evolves into a nearly triangular pattern with increasing powers (i.e., associated with larger spectra). However, for an input power of 32 mW, we clearly distinguish the formation of a localized short temporal structure within each period of the initial beating, in contrast with the normal dispersion regime. However, at input powers exceeding 50 mW, a noticeable decline in the intensity coherence of the temporal pattern is observed, directly attributed to the detrimental impact of MI, as depicted in Figure 3a. The reduced contrast between the central autocorrelation peak and the neighboring intercorrelation peaks in the signal exposes a pronounced jitter in the pulse train, related to coherence loss of the multi-line comb source.

4 Experimental results at 2 μm

Thanks to the simple architecture of our system, we extended this work to the 2-μm waveband by interchanging suitable fiber components and pump lasers. Due to the high linear losses of silica-based fibers in this spectral range, we used the shorter normally-dispersive HNLF (length equal to 350 m), which still exhibits normal dispersion (β_2 ~ 1 ps^2/km) around 1.95–2.0 μm. The nonlinear coefficient was estimated to be ~8 W^{-1}·km^{-1}. More details about the Brillouin properties at 2-μm pump wavelength of similar fibers can be found in Ref. [26]. We first measured the dual-frequency Brillouin lasing threshold by extracting only 1% of the optical cavity power as a function of the injected pump power. As shown in Figure 4a, an input power of 90 mW allowed us to reach the dual-frequency Stokes lasing in our ring cavity in the case of a frequency spacing of 106 GHz (0.85 nm) around 1.98 μm. In Figure 4b,

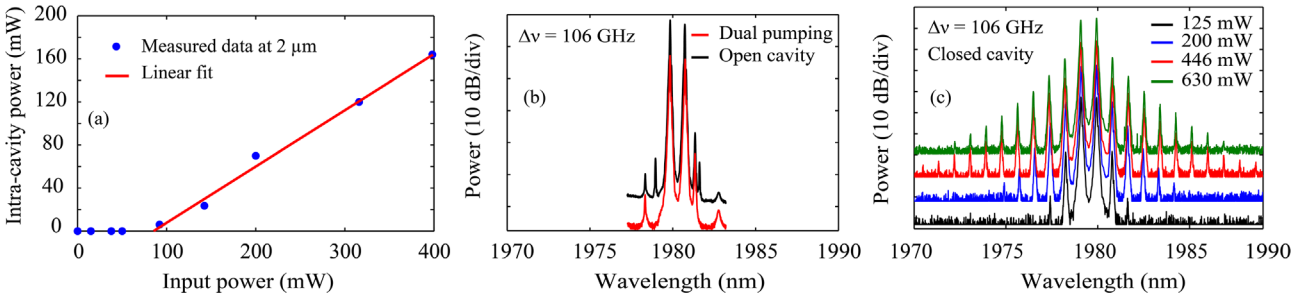

Fig. 4. Dual-frequency Brillouin lasing and multi-wavelength light generation in a multimode regime in the 2-μm waveband. (a) Stokes laser threshold measurement. (b) Experimental recording with 106 GHz frequency spacing of the dual pumping and cavity-free FWM configuration at 200 mW pomp power. (c) Experimental FWM results as a function of the injected power at fixed pumps frequency of 106 GHz in close cavity configuration.

the experimental spectrum of the initial dual-frequency pumping is illustrated alongside the corresponding output of the HNLF fiber (i.e., open cavity configuration) for an input power of 200 mW. Because of the higher fiber losses at such wavelengths (about 15 dB/km), the cascaded FWM process proves to be highly inefficient in this cavity-free configuration, failing to generate any new spectral lines. This outcome persists despite the judicious selection of this fiber due to its moderate losses compared to typical silica fibers. It becomes here obvious that our closed cavity configuration based on the dual-frequency Brillouin laser will provide an interesting solution for MFWM processes and the generation of a multi-wavelength light source. Figure 4c confirms this claim by showing the spectral broadening obtained in the cavity upon increasing input powers from 125 mW to 630 mW. As previously shown, the cavity operating in the normal dispersion does not present any saturation of MFWM due to MI. The number of comb lines increases rapidly to 22 lines when the input power reaches 446 mW. Furthermore, within this specific range of a few hundred milliwatts, we observe a spectral saturation, mirroring the behavior observed in the 1.55-μm experiment. It is important to note that the generated comb lines are fewer in number compared to those at 1.55 μm, primarily due to the higher cavity losses, exhibiting an order of magnitude difference.

5 Conclusion

In conclusion, despite employing extended cavity lengths in the dual-frequency Brillouin fiber laser, resulting in multimodal laser operation, we have experimentally confirmed the effective generation of multiwavelength comb sources through cascaded four-wave mixing (FWM) processes at both 1.55 μm (C-band) and 2 μm (thulium band). We have shown that the number of comb lines undergoes rapid expansion with increasing input power, and their frequency spacing is adjustable by varying the initial pump wavelengths. Additionally, distinct characteristics related to the sign of net cavity dispersion were also evidenced. While this long-cavity configuration was previously examined at 1.55 μm in Ref. [23], it was limited to one dispersion regime, without emphasizing the adverse effects of MI. Notably, we did not specifically optimize fiber cavity lengths for coherent comb generation in this study. For further insights into this aspect, we direct the reader to previous works conducted at 1.55 μm [24, 27].

Furthermore, we extended the approach to the 2-μm waveband, where cascaded FWM in the continuous-wave regime is typically impeded by significant fiber losses. No asymmetric spectral broadenings were observed when initial power is equally distributed over the two pumps, since we were operating in a free-running configuration without a phase-locking loop scheme (in contrast with Ref. [24], where pump detuning is effectively controlled). Nevertheless, the enhanced performances of cascaded FWM in this simple architecture of the Brillouin fiber laser make it readily applicable at any wavelength where fiber components and CW lasers are available. A straightforward application in the future could extend in the mid-infrared region, leveraging fluoride glass fiber or chalcogenide fiber technology, but also in the high-demanding 1-μm waveband. However, to maintain the complete coherence properties of the generated combs, the implementation of a stabilization scheme is necessary, as recently demonstrated at 1 μm [28].

Funding

The authors acknowledge the support of the Agence Nationale de la Recherche (Grant Number: ANR-16-CE24-0010, ANR-17-EURE-0002, ANR-15-IDEX-0003), the Conseil Régional de Bourgogne Franche-Comté and the European Framework Programme (Grant 101135904).

Conflicts of interest

The authors declare no conflict of interests.

Data availability statement

Data underlying the results presented in this paper are not publicly available at this time but may be obtained from the authors upon reasonable request.

Author contribution statement

All authors made significant contributions to this work.

References

1 Cossel K.C., Waxman E.M., Finneran I.A., Blake G.A., Ye J., Newbury N.R. (2017) Gas-phase broadband spectroscopy using active sources: progress, status, and applications [Invited], *J. Opt. Soc. Am. B* **34**, 1, 104–129.

2 Russell E., Corbett B., Gunning F.C.G. (2022) Gain-switched dual frequency comb at 2 μm, *Opt. Express* **30**, 4, 5213–5221.

3 Parriaux A., Hammani K., Millot G. (2018) Two-micron all-fibered dual-comb spectrometer based on electro-optic modulators and wavelength conversion, *Commun. Phys.* **1**, 1, 1–7.

4 Cao W., Hagan D., Thomson D.J., Nedeljkovic M., Littlejohns C.G., Knights A., Alam S.-U., Wang J., Gardes F., Zhang W., Liu S., Li K., Rouifed M.S., Xin G., Wang W., Wang H., Reed G.T., Mashanovich G.Z. (2018) High-speed silicon modulators for the 2 μm wavelength band, *Optica* **5**, 9, 1055–1062.

5 Gunning F., Corbett B. (2019) Time to open the 2-μm window?, *Opt. Photonics News* **30**, 3, 42–47.

6 Dada A.C., Kaniewski J., Gawith C., Lavery M., Hadfield R. H., Faccio D., Clerici M. (2021) Near-maximal two-photon entanglement for optical quantum communication at 2.1 μm, *Phys. Rev. Appl.* **16**, 5, L051005.

7 Parriaux A., Hammani K., Millot G. (2020) Electro-optic frequency combs, *Adv. Opt. Photonics* **12**, 1, 223–287.

8 Kayes M.I., Rochette M. (2017) Optical frequency comb generation with ultra-narrow spectral lines, *Opt. Lett.* **42**, 14, 2718–2721.

9 Wu R., Supradeepa V.R., Long C.M., Leaird D.E., Weiner A.M. (2010) Generation of very flat optical frequency combs from continuous-wave lasers using cascaded intensity and phase modulators driven by tailored radio frequency waveforms, *Opt. Lett.* **35**, 19, 3234–3236.

10 Washburn B.R., Diddams S.A., Newbury N.R., Nicholson J. W., Yan M.F., Jørgensen C.G. (2004) Phase-locked, erbium-fiber-laser-based frequency comb in the near infrared, *Opt. Lett.* **29**, 3, 250–252.

11 Cundiff S.T., Ye J. (2003) Colloquium: Femtosecond optical frequency combs, *Rev. Mod. Phys.* **75**, 1, 325–342.

12 Del'Haye P., Schliesser A., Arcizet O., Wilken T., Holzwarth R., Kippenberg T.J. (2007) Optical frequency comb generation from a monolithic microresonator, *Nature* **450**, 7173, 1214–1217.

13 Kippenberg T.J., Holzwarth R., Diddams S.A. (2011) Microresonator-based optical frequency combs, *Science* **332**, 6029, 555–559.

14 Xing S., Kowligy A.S., Lesko D.M.B., Lind A.J., Diddams S. A. (2020) All-fiber frequency comb at 2 μm providing 1.4-cycle pulses, *Opt. Lett.* **45**, 9, 2660–2663.

15 Wang X., Jia K., Chen M., Cheng S., Ni X., Guo J., Li Y., Liu H., Hao L., Ning J., Zhao G., Lv X., Huang S.-W., Xie Z., Zhu S.-N. (2022) 2 μm optical frequency comb generation via optical parametric oscillation from a lithium niobate optical superlattice box resonator, *Photonics Res.* **10**, 2, 509–515.

16 Hu K., Kabakova I.V., Lefrancois S., Hudson D.D., He S., Eggleton B.J. (2014) Hybrid Brillouin/thulium multiwavelength fiber laser with switchable single- and double-Brillouin-frequency spacing, *Opt. Express* **22**, 26, 31884–31892.

17 Zhao S., Lu P., Liu D., Zhang J. (2013) Switchable multiwavelength thulium-doped fiber ring lasers, *Opt. Eng.* **52**, 8 086105.

18 Wang X., Zhu Y., Zhou P., Wang X., Xiao H., Si L. (2013) Tunable, multiwavelength Tm-doped fiber laser based on polarization rotation and four-wave-mixing effect, *Opt. Express* **21**, 22, 25977–25984.

19 Peng W., Yan F., Li Q., Liu S., Feng T., Tan S. (2013) A 1.97 μm multiwavelength thulium-doped silica fiber laser based on a nonlinear amplifier loop mirror, *Laser Phys. Lett.* **10**, 11 115102.

20 Jiang S., Guo C., Fu H., Che K., Xu H., Cai Z. (2020) Mid-infrared Raman lasers and Kerr-frequency combs from an all-silica narrow-linewidth microresonator/fiber laser system, *Opt. Express* **28**, 25, 38304–38316.

21 Fatome J., Pitois S., Fortier C., Kibler B., Finot C., Millot G., Courde C., Lintz M., Samain E. (2010) Multiple four-wave mixing in optical fibers: 1.5–3.4-THz femtosecond pulse sources and real-time monitoring of a 20-GHz picosecond source, *Opt. Commun.* **283**, 11, 2425–2429.

22 Wolff C., Smith M.J.A., Stiller B., Poulton C.G. (2021) Brillouin scattering – theory and experiment: tutorial, *J. Opt. Soc. Am. B* **38**, 4, 1243–1269.

23 Li Q., Jia Z., Li Z., Yang Y., Xiao J., Chen S., Qin G., Huang Y., Qin W. (2017) Optical frequency combs generated by four-wave mixing in a dual wavelength Brillouin laser cavity, *AIP Adv.* **7**, 7, 075215.

24 Lucas E., Deroh M., Kibler B. (2023) Dynamic interplay between Kerr combs and Brillouin lasing in fiber cavities, *Laser Photonics Rev.* **17**, 12, 2300041.

25 Bai Y., Zhang M., Shi Q., Ding S., Qin Y., Xie Z., Jiang X., Xiao M. (2021) Brillouin-Kerr soliton frequency combs in an optical microresonator, *Phys. Rev. Lett.* **126**, 6 063901.

26 Deroh M., Beugnot J.-C., Hammani K., Finot C., Fatome J., Smektala F., Maillotte H., Sylvestre T., Kibler B. (2020) Comparative analysis of stimulated Brillouin scattering at 2 μm in various infrared glass-based optical fibers, *J. Opt. Soc. Am. B* **37**, 12, 3792–3800.

27 Deroh M., Lucas E., Kibler B. (2023) Dispersion engineering in a Brillouin fiber laser cavity for Kerr frequency comb formation, *Opt. Lett.* **48**, 24, 6388–6391.

28 Deroh M., Lucas E., Hammani K., Millot G., Kibler B. (2023) Stabilized single-frequency sub-kHz linewidth Brillouin fiber laser cavity operating at 1 μm, *Appl. Opt.* **62**, 30, 8109–8114.